remote sensing

MDPI

Article

Inside Late Bronze Age Settlements in NE Romania: GIS-Based Surface Characterization of Ashmound Structures Using Airborne Laser Scanning and Aerial Photography Techniques

Casandra Brașoveanu [1], Alin Mihu-Pintilie [1,*] and Radu-Alexandru Brunchi [2]

[1] Department of Exact and Natural Sciences, Institute of Interdisciplinary Research, Alexandru Ioan Cuza University of Iași (UAIC), St. Lascăr Catargi 54, 700107 Iasi, Romania; casandra.brasoveanu@uaic.ro or brasoveanu.casandra@yahoo.com

[2] Doctoral School, Faculty of History, Alexandru Ioan Cuza University of Iași (UAIC), St. Lascăr Catargi 54, 700107 Iasi, Romania; radu.brunchi@uaic.ro or radubrun-chi@gmail.com

* Correspondence: mihu.pintilie.alin@gmail.com or alin.mihu.pintilie@uaic.ro; Tel.: +40-741-912-245

Abstract: The identification and delineation, through aerial photography, of the archaeological structures that present temporal resolution, as well as their characterization based on high-resolution LiDAR (Light Detection and Ranging)-derived DEMs (Digital Elevation Models) are modern techniques widely used in the archaeological prospecting of various landscapes. In this study, we present an application of Airborne Laser Scanning (ALS) and aerial photography (AP) techniques, used in order to compute geomorphometric indices specific to the ashmound structures of Late Bronze Age (LBA) archaeological sites that are visible on the soil surface. The necessity of determining the ashmounds' geoarchaeological description stems from the fact that despite the majority of archaeologists weighing in on the subject, there is still no accepted explanation regarding their initial functionality. Thus, we believe that the GIS-based high-resolution characterization of 200 ashmound features identified in 21 Noua Culture (NC) archaeological sites will contribute to a better understanding of the ashmounds' functionality and evolution in the heterogeneous landscape of the study area (NE Romania). Therefore, various shape indices, such as the area (A), perimeter (P), length (L), form factor (RF), circularity ratio (RC), and elongation ratio (RE) were computed for microlevel characterizations of the visible ashmounds' structures. Additionally, LiDAR-derived DEMs with a 0.5 m resolution were used to generate more surface characteristics such as the slope (S) and hypsometric indices (HI). The outcomes indicate that the ashmounds have relatively diverse shapes (an RF range from 0.37 to 0.77; a RC range from 0.79 to 0.99; a RE range from 0.68 to 0.99), and the micro-relief slightly varies from positive to negative landforms (HI range from 0.34 to 0.61) depending on the erosion intensity (S range from 1.17° to 19.69°) and anthropogenic impact (e.g., current land use and agriculture type). Furthermore, each morphometric parameter is an indicator for surface processes, aiding in the identification of the geomorphologic and surface-erosion aspects that affect the archaeological remains, contributing to the assessment of the conservation status of the ashmound structures within the current landscape configuration. In this regard, this article presents and discusses the remote sensing (RS) techniques used, as well as the morphometric data obtained, exploring the implications of our findings for a better characterization of the NC in Romania.

Keywords: GIS; airborne laser scanning (ALS); aerial photography (AP); ashmound archaeological structures; temporal resolution; Noua Culture—Late Bronze Age (NC-LBA); NE Romania

Citation: Brașoveanu, C.; Mihu-Pintilie, A.; Brunchi, R.-A. Inside Late Bronze Age Settlements in NE Romania: GIS-Based Surface Characterization of Ashmound Structures Using Airborne Laser Scanning and Aerial Photography Techniques. *Remote Sens.* **2023**, *15*, 4124. https://doi.org/10.3390/rs15174124

Academic Editor: Fulong Chen

Received: 29 June 2023
Revised: 11 August 2023
Accepted: 18 August 2023
Published: 22 August 2023

1. Introduction

During the last few decades, geoarchaeological investigations, such as the pollen-based analysis of sedimentary sequences, have allowed the identification of significant climatic oscillations that occurred during the second part of the Subboreal period during two chronological sequences, namely 4000–3600 cal BP and 3200–3000 cal BP [1]. The

consequences for prehistoric communities were substantial, representing the primary reasons behind the transformations that took place at the end of the Bronze Age (BA) [2]. In this context, in the northwestern Pontic (Black Sea) region, the agricultural communities of the Middle Bronze Age (MBA) were gradually replaced by human groups characterized by a predominantly pastoral economy [3,4], and these changes had effects on multiple levels.

In this framework, our investigation focuses on the emergence of a new type of settlement that presents a temporal resolution (visible only outside of the growing season), considered to be an important cultural marker for the pastoralist communities of the Late Bronze Age (LBA), namely the Noua-Sabatinovka-Coslogeni (NSC) cultural complex [5,6]. The latter occupied a wide area, extending from the territory located east of the Apuseni Mountains (Western Romanian Carpathians) in Romania up to the Dnieper region, and from Ukraine's sub-Carpathians up to northeastern Bulgaria (Danube Valley) [7]. Among the similar characteristics of the three cultures that compose this complex, we have to mention the preference for an economy based on animal husbandry (especially cattle), a quasiuniform typology of the ceramic forms utilized (e.g., jar/bag vessels, decorated with simple strips of clay; cups with one or two raised handles), the usage of numerous flint (e.g., *krummesser* and arrowheads) and bone (e.g., crenated *scapulae*, *tupik* sickles and needles) tools, and, most importantly, the presence of the settlements with *ashmounds* (quasicircular grey spots visible on the soil surface with diameters between 15 and 45 m and small elevations, resembling small mounds) [5–10].

The ashmounds, also known as *ash heaps*, *cinder mounds*, or *zolniki*, were first discovered and described at the end of the 19th century by Zaretskyi [11] and at the beginning of the 20th century by Gorodčov [12]. Initially, they were believed to be special places destined for votive offerings or the remains of cremation barrows belonging to Iron Age (IA) settlements, in particular Scythian settlements [13]. However, later on, in the mid-20th century, these features were identified within sites belonging to the NSC cultural complex [14] and the Belogrudovka culture [15]. The term *ashmound* was first coined to describe the characteristics of the Scythian settlement of Bel'sk [12], and it was named based on its appearance, as these 'structures' were long believed to represent ashes due to their light-grey color. After decades of discussions, it is now a known fact that no form of burning was involved in producing the ash-like soil [9,10,15–19]. However, a single accepted explanation for the ashmounds' functionality is still missing, despite the vast majority of specialists weighing in on the subject. The ashmound features are easily identifiable outside the growing season due to their distinct soil marks and elevation, making them visible on orthophotos, satellite images, LiDAR (Light Detection and Ranging) measurements, and aerial photographs [7]. These methods are essential for archaeology, allowing: the identification of new sites; detailed studies of the areas where human groups once settled; and site documentation, monitoring, and interpretation [20–26]. Although the importance of these methods has constantly been proven in different studies concerning the prehistoric communities that inhabited latter-day Romania [27–32], when talking about the LBA or NSC cultural complex, the studies utilizing detailed RS methods and products (e.g., high-resolution DEMs or aerial photographs) are relatively few [33–36].

In this study, we aim to address the gap related to the high-resolution investigation of the ashmounds by providing the first GIS-based surface characterization of 200 ashmound features identified in 21 Noua Culture (NC) archeological sites from northeastern Romania by using Airborne Laser Scanning (ALS) and aerial photography (AP) techniques. Our main goals are (i) to highlight the role of the GIS-based surface characterization of the ashmound features as a crucial tool for understanding the habitation behavior and ecocultural evolution of prehistoric communities belonging to NC during the LBA, and (ii) to characterize the conservation status of the ashmound structures in the current landscape configuration of northeastern Romania. In light of these goals, we present and discuss the RS techniques used and the morphometric data obtained and further explore the implications of our findings for a better characterization of the LBA communities known as Noua culture.

2. Study Area

2.1. Geoarchaeological Framework

The study area is located in the northeastern part of Romania, encompassing the territory of the middle and lower Jijia catchment [37] (Figure 1). The Jijia River is the primary tributary of the Prut River, serving as the natural border between Romania and the Republic of Moldova [38,39]. Broadly, the entire area is commonly known as the Moldavian Plain, but a more accurate name would be the Jijia Hills due to the fact that it is a hilly region, which coincides with the central northeastern part of the Moldavian Plateau [40,41]. The elevation ranges from 40 m to 256.5 m, with an average elevation of 112 m. Altitudes above 200 m indicate the contact area between the Jijia Hills and the Central Moldavian Plateau on the southern flank, as well as the contact area between the Jijia Hills and the Suceava Plateau on the western flank. Elevations below 50 m correspond to the shared floodplain of the Jijia and Prut rivers in the southeast. The slope ranges from flat areas like major floodplains and structural plates to 88.5° (mean slope of 5.37°), with the highest values observed especially on the front of the cuestas affected by landslides and on the active banks of the large rivers (e.g., Prut and Jijia) [41]. The climate is temperate continental, with an average annual temperature ranging between 8 and 10 °C and an annual mean precipitation value ranging from 450 mm to 500 mm [7].

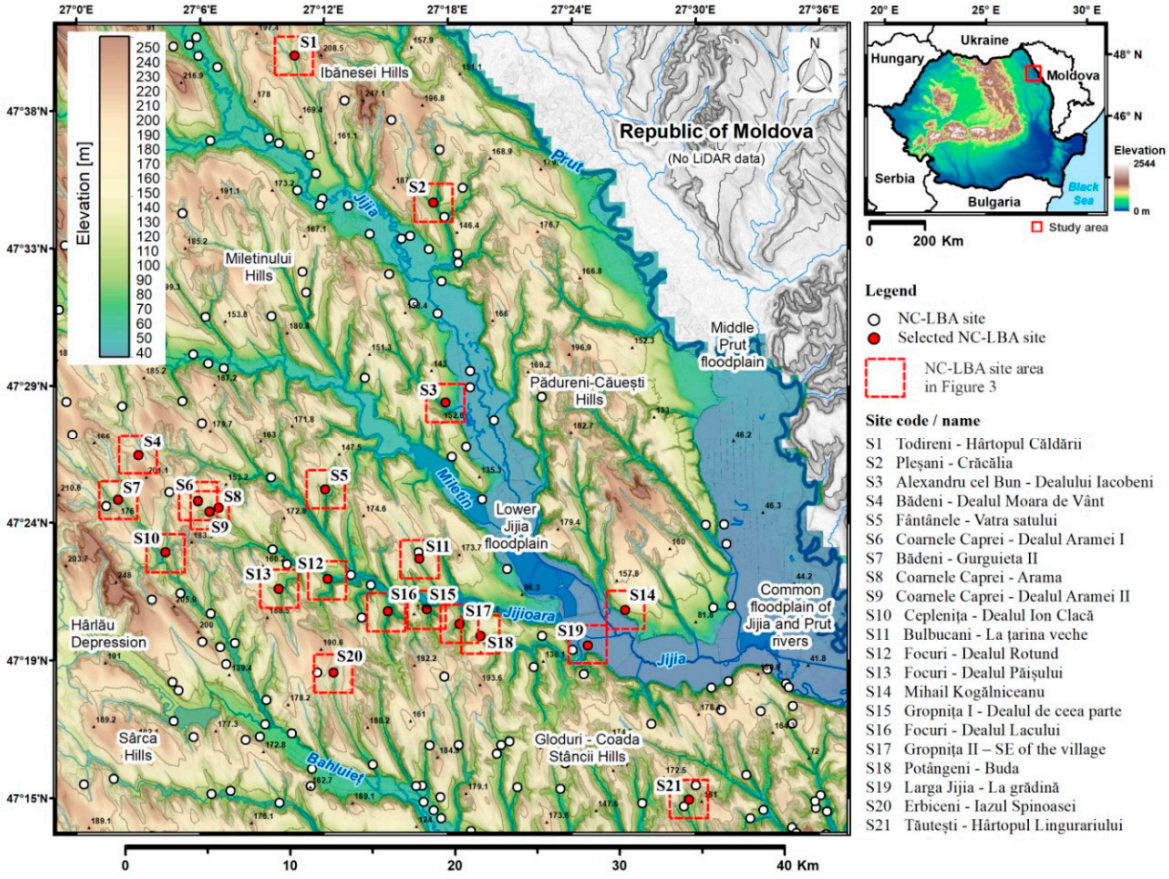

Figure 1. Geographic location of the study area (Jijia Hills) within Romania and the distribution of the selected NC-LBA sites (see Table S1); the number of ashmound structures identified within each NC-LBA site are indicated.

The lithological structure of the entire region is a monocline specific to the Moldavian Plateau, with Miocene–Pleistocene dipping strata from northwest to southeast, respectively, from the Suceava Plateau to the middle Prut floodplain and the common floodplain of the Jijia and Prut rivers [40]. The geological structure comprises the succession of sandy clay deposits (200–300 m thickness) and layers of limestone and sandstone from the Lower and

Medium Sarmatian age (2–30 m thickness) overlaid by a loess stratum with thicknesses ranging from 1–2.5 m to 15–30 m (e.g., river terraces) [42]. The major valleys of the Prut, Jijia, Miletin, Jijioara, and Bahlui rivers are characterized by Holocene alluvial deposits, with the lower sector of the Jijia floodplain (3.5 km wide max.) and the middle sector of Prut Valley (7.5 wide max.) being the most developed in the landscape [43]. The dominant landforms in the heterogeneous landscape of the study area are the large valleys separated by interfluves that are mostly of the cuesta type. According to the previous studies [7,40], the cuestas along with the open slopes and local hills in valleys are the main landforms preferred by prehistoric populations to establish their settlements.

The workspace, namely the Jijia Hills region from NE Romania, was chosen to perform the current study due to its extensive habitation during prehistoric periods, including the Chalcolithic (Precucuteni/Cucuteni–Trypillia cultural complex) [29,30,44] and Bronze Age (BA) [7,34]. The high density of cultural heritage found throughout the entire territory of Jijia Hills serves as evidence of the essential physical–geographical characteristics that describe this region, making it suitable for the development of communities, both in historical as well as in present times. Therefore, the chronological framework selected in this study is the LBA (1600–1100 cal BP). This choice is mainly due to the significant number of archaeological discoveries belonging to this chronological stage, but also because, to this day, relatively few modern studies have been dedicated to this prehistoric period. Also, the LBA workspace was highly frequented by human groups belonging to the Noua Culture (NC), resulting in over 400 archaeological sites such as settlements, necropolises, and hoards being left behind [34].

2.2. Noua Culture (LBA) Habitation in NE Romania

In the modern territory of Romania, the LBA can be described as the stage in which the previous archaeological cultures, dating from the MBA, were continued and ended and, most importantly, as the emergence period of two important cultural complexes: Noua-Sabatinovka-Coslogeni (NSC) and Zimnicea–Plovdiv. The last two have appeared as a result of the contacts existing between the local communities and the eastern and southern elements [4,6,14].

As we have already stated, the focus of our paper is on the human groups belonging to Noua Culture (NC). While the sites specific for these communities can also be found in Ukraine, the Republic of Moldova, and other territories of Romania (e.g., Transylvania), the selected workspace is considered to be the most important region of NC development, benefiting from the highest number of discoveries [13] consisting mostly of settlements. The latter can be categorized into two types in accordance with the presence or absence of the ashmounds on the soil surface. While many theories have been postulated regarding the differentiation existing between the two types of sites [13,18,19,45], a satisfactory answer is still missing. In this regard, recent studies [7,34] have brought to light an important aspect, namely the possibility that the ashmounds with very good soil contrast and small-to-no elevations could be, in fact, a consequence of intensive agricultural works. In addition, after performing test trenches in a settlement without such features visible, Dascălu [45] was able to prove the presence of the ashmound feature beneath the arable soil layer. Thus, the current state of research seems to be far from satisfactory enough to allow the issuance of theories regarding the functionality of the ashmounds or the behavior of NC communities (Figure 2). Therefore, in order to achieve the objectives of our study, 21 NC sites with ashmounds from Jijia Hills (NE Romania) (Figure 1) were selected, presenting between two and nineteen such features, located mostly in the southern half of the workspace (Table 1). During our previous studies [7,34] and projects, we conducted numerous field surveys within settlements of this type throughout the entire area of interest, but for this paper, we chose as case studies only the most relevant situations, with high contrasting soil marks and an important amount of archaeological material discovered.

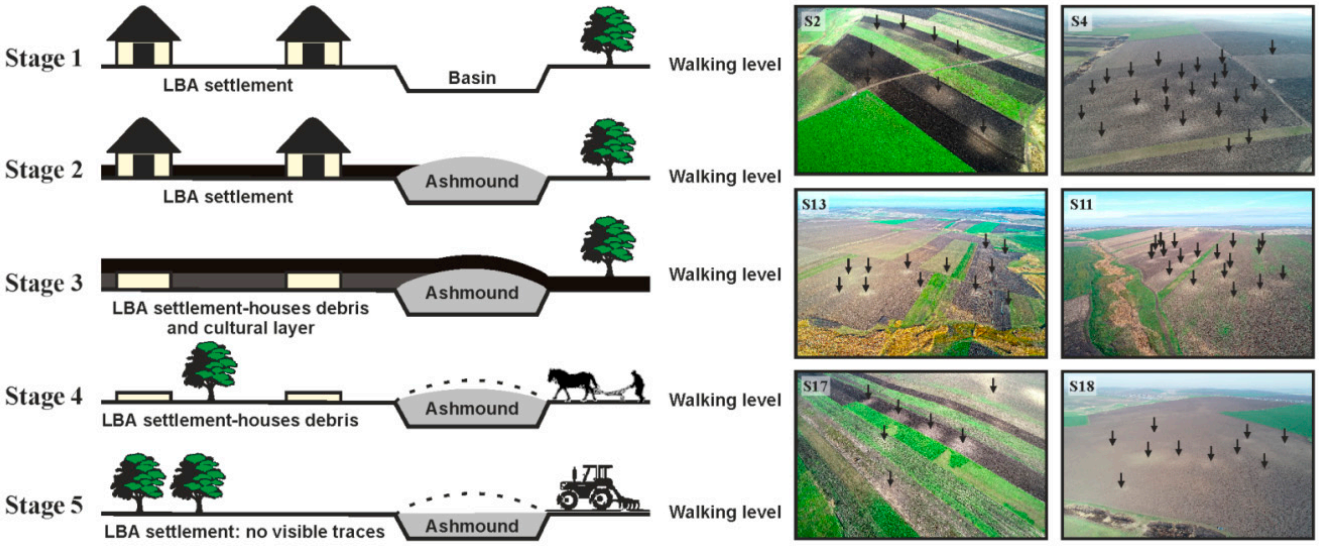

Figure 2. The supposed evolution stages of a NC settlement with ashmounds, redrawn after Dietrich [9]: Stage 1—the ashmound basin construction phase; Stage 2—the phase where the basin slowly fills up with waste and debris and the ashmound reaches its maximum height; Stage 3—the conservation stage of the ashmound due to new cultural layers and/or soil accumulation on top; Stage 4—the first erosion phase, which affects both older soil layer and the ashmound structure; Stage 5—the second erosion phase when the destruction of the upper settlement layers is almost complete and only the ashmound basin remains. In the oblique images (right photos), the ashmound structures are highlighted with arrows (light-grey 'spots' on soil) from different NC sites.

Table 1. List of the 21 NC-LBA archaeological sites (see Figure 1 and Table S1) analyzed in this work and their main feature characteristics. S1 to S21 are the site Ids. For the computation of landform classes corresponding to the location of the NC-LBA sites, please refer to our previous articles [7,40].

Id	Site Name	Lat. N	Long. E	Elevation (m a.s.l.)	Area (ha)	Landform Corresponding to NC-LBA Sites [1]	Number of Visible Ashmounds
S1	Todireni—Hârtopul Căldării	47.41	27.02	109.9	8.9	Local ridges/hills in valley	16
S2	Pleșani—Cracalia	47.35	27.24	82.0	5.1	Local ridges/hills in valley	10
S3	Alexandru cel Bun—Dealul Iacobeni	47.35	27.27	76.8	7.6	Hill tops, high ridges	2
S4	Bădeni—Dealul Moara de Vânt	47.34	27.29	168.5	11	Hill tops, high ridges	16
S5	Fântânele—Vatra Satului	47.32	27.40	106.7	16.6	Local ridges/hills in valley	13
S6	Coarnele Caprei—Dealul Aramei I	47.34	27.43	140.2	7.2	Upper slopes	8
S7	Bădeni—Gurguieta II	47.57	27.28	98.2	4.8	U-shaped valleys	6
S8	Coarnele Caprei—Arama	47.65	27.17	126.9	4.1	Hill tops, high ridges	7
S9	Coarnele Caprei—Dealul Aramei II	47.41	27.09	103.8	4.8	Local ridges/hills in valley	5
S10	Ceplenița—Dealul Ion Clacă	47.46	27.29	94.5	8.4	U-shaped valleys	11
S11	Bulbucani—La țarina veche	47.33	27.31	101.7	10.1	Deeply incised streams	19
S12	Focuri—Dealul Rotund	47.41	27.10	72.4	3.6	Deeply incised streams	5
S13	Focuri—Dealul Păișului	47.24	27.47	87.9	15.7	U-shaped valleys	13
S14	Mihail Kogălniceanu	47.44	27.04	94.9	9.2	Hill tops, high ridges	4
S15	Gropnița I—Dealul de ceea parte	47.37	27.26	64.8	3.7	Deeply incised streams	10
S16	Focuri—Dealul Lacului	47.38	27.06	65.9	2.8	Deeply incised streams	9
S17	Gropnița II—SE of the village	47.40	27.10	65.8	3.7	Deeply incised streams	10
S18	Potângeni—Buda	47.31	27.19	95.2	7.3	Deeply incised streams	5
S19	Larga Jijia—La grădină	47.41	27.19	45.0	5.3	U-shaped valleys	5
S20	Erbiceni—Iazul Spinoasei	47.36	27.15	113.7	8.1	Deeply incised streams	16
S21	Tăutești—Hârtopul Lingurariului	47.37	27.19	101.4	7.2	Local ridges/hills in valley	10

[1] Landform classes adapted after [40] for specific landscape characteristics of the study area [7].

3. Data Acquisition and Methodology

Figure 3 summarizes the workflow chart adhered to in this study, encompassing: the LBA settlements inventory and NC site selection; the field investigation employing oblique and vertical aerial photography; as well as the ALS survey, the acquisition process of the

GIS data, and the computation of morphometric indices to characterize the surface features of the ashmound structures. Subsequent sections will detail each of these methodological steps.

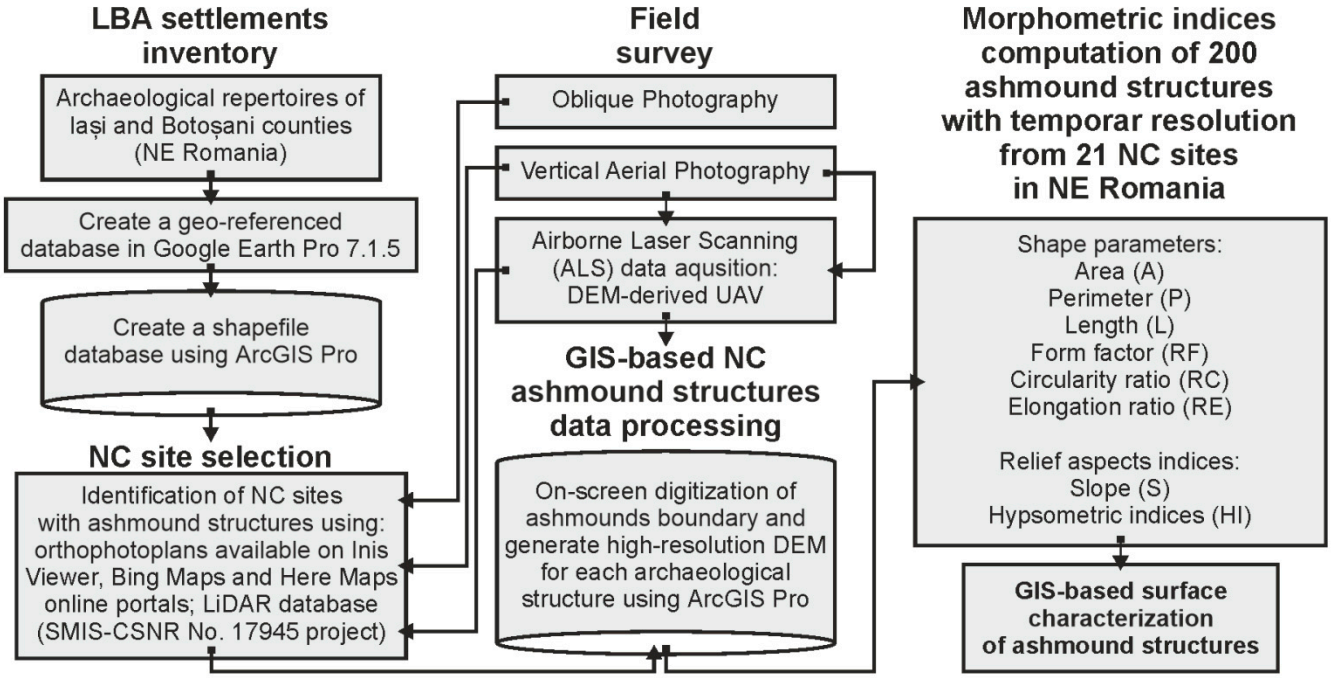

Figure 3. Workflow chart followed in this study of GIS-based surface characterization of the 200 ashmound structures with temporal resolution, identified across 21 NC sites in NE Romania.

3.1. LBA Settlements Inventory and NC Site Selection

The NC-LBA sites inventory was compiled firstly by consulting the archaeological repertoires [5,46–49]. In addition, due to the partial visibility of the ashmound structures on the topographic surface, we were able to identify a significant number of novel sites [34] by using the LiDAR database [50]; aerial photographs; and the orthophotos available on different portals, such as Inis Viewer, Bing Maps, and Here Maps. The georeferenced database was generated in Google Earth Pro 7.1.5 and exported as a shapefile in ArcGIS Pro [7]. An Id (code) was attributed to the selected sites (S1-S21) following the N-S axis (Table 1 and Table S1). In all cases, the settlements are located in close proximity to secondary water courses or near to the confluence with other streams [7].

Thus, S1 is represented by the settlement from Todireni—Hârtopul Căldării (Botoșani County) that occupies an area of approx. 9 ha, being located at the confluence of Mihăiasa Valley and one of its tributaries. S2 is the site of Pleșani—Cracalia (Botoșani County), of ca. 5 ha, placed at the confluence of Glăvănești Valley and one of its secondary tributaries. S3, Alexandru cel Bun—Dealul Iacobeni (Iași County), was discovered on the SSW slope of Iacobeni Hill in the proximity of Aluza River. S4 is represented by Bădeni—Dealul Moara de Vânt (Iași County), a settlement of 11 ha, with 16 ashmounds visible that were found on the NNE slopes of Moara de Vânt Hill near the river with the same name. The latter separates the site into two distinct areas: one with fifteen clustered ashmounds and another with at least one such feature. This aspect has been signaled in other sites as well [8,13], with the ashmounds being organized in groups and divided in the present time by a small gully. S5, the site of Fântânele—Vatra Satului (Iași County), occupies a larger surface of approx. 16 ha, although it has a smaller number of ashmounds visible (13). It is located on the SW slope of Ciorii Hill, near Clătinici Valley (Table 1; Figure 4).

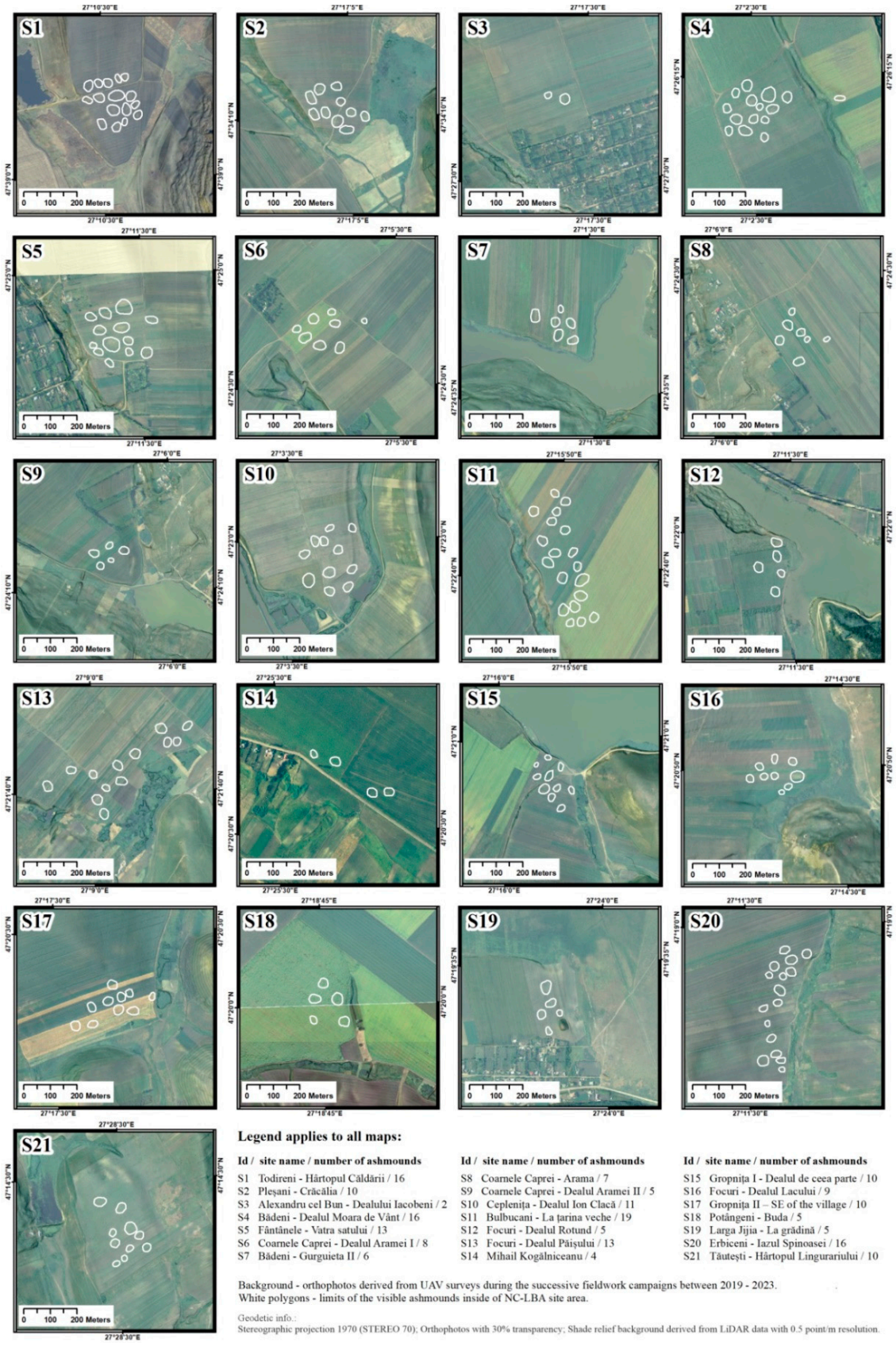

Figure 4. The NC-LBA sites area (see Figure 1 and Table S1) in which the ashmounds are indicated with white polygons.

S6 and S9, Coarnele Caprei—Dealul Aramei I and II (Iași County), are located on the slopes of Aramei Hill, near Puig River. The sites occupy surfaces of 7 ha and 5 ha, respectively, having between 5 and 8 visible ashmounds. S7 is the site of Bădeni—Gurguieta II (Iași County), located on the S slope of Boului Hill near Gurguieta River, and occupies ca. 5 ha, with 6 ashmounds visible on the soil surface. S8, Coarnele Caprei—Arama (Iași County), is placed in the proximity of the two settlements from Aramei Hill (S6 and S9), being located near Pais River on the SSW slope of Bahniței Hill on an area of approx. 4 ha and having 7 visible ashmounds (Table 1; Figure 4).

Regarding S10, Ceplenița—Dealul Ion Clacă (Iași County), it is found on the S slope of Ion Clacă Hill, near Urechii pond, on a surface of 8 ha. Next, S11 is represented by the site from Bulbucani—La țarina veche (Iași County), one of the biggest settlements in regard to the number of visible ashmounds (19). It is placed on the western slopes of Crucii Hill near Boziana Valley. S12 (Focuri—Dealul Rotund, Iași County) is one of the smallest settlements (3.6 ha), being located on the E slopes of Rotund Hill with 5 visible ashmounds. S13 is the site of Focuri—Dealul Păișului (Iași County), which occupies an area of approx. 15 ha, being located at the confluence of Barboșica Valley and one of its tributaries. S14 is the site from Mihail Kogălniceanu—E of the village (Iași County), consisting of 4 ashmounds occupying ca. 9 ha of the W slope of Bășești Hill and in close proximity to Jijia Valley. S15, Gropnița—Dealul de ceea parte (Iași County), is placed on the E slope of Morii Hill, near Herghetea Valley (Table 1; Figure 4).

S16, Focuri—Dealul Lacului (Iași County), is located on the E slope of Lacului Hill near Lacul Negru Valley, occupying approx. 3 ha. S17, Gropnița—SE of the village (Iași County), is also a small site, occupying less than 4 ha, but it presents 10 ashmounds on the soil surface, being located in a confluence area on the SSE slopes of the hill found S of Gropnița village. S18 is the site of Potângeni—Buda (Iași County), with 5 ashmounds in an area of ca. 7 ha placed at the confluence of Buda River and one of its tributaries. Larga Jijia—La grădină (S19) was discovered in the proximity of the Jijia River. The 5 ashmounds that compose the site are surrounding a burial mound that was probably "raised" during the Early BA, occupying approx. 5 ha. S20, Erbiceni—Iazul Spinoasei (Iași county), is represented by 16 ashmounds identified on an area of ca. 8 ha, located in the immediate vicinity of Valea Lungă River. Finally, S21 is the site of Tătuești—Hârtopul Lingurariului (Iași County), placed on the SW slopes located between the rivers Valea Prisăcii and Valea Apărești, with 10 ashmounds, noticeable on approx. 7 ha (Table 1; Figure 4).

3.2. Airborne Laser Scanning (ALS) Data

The Digital Elevation Model (DEM) derived from ALS (Airborne Laser Scanning) [30,51] surveys provides the most detailed information regarding the microtopography of surface ashmound structures [7] compared to other DEMs derived from topographic maps (1:25,000 scale) and plans (1:5000 or 1:2000 scale) or SRTM-derived DEMs (30 m cell size) that were frequently used in previous archaeological studies [52]. Therefore, the NC ashmounds' DEMs used in this work were extracted from a high-density LiDAR database acquired by using a Leica ALS60 system within the SMIS-CSNR No. 17945 project [53], which was coordinated by the Prut–Bîrlad Water Administration (PBWA) in northeastern Romania [7,37,39,54]. The point cloud data, which cover more than 21,000 km^2, were classified and converted to ASPRS 1.1 format classes [53]. The data georeferencing was achieved by using a network of 387 geodetic points measured in both ERTS89 and Stereo 70 geographical projections, for which a quasigeoid model was computed [31]. The LiDAR point density ranged from 2 to 6 points/1 m^2, depending on the land cover type. The point cloud was filtered to exclude vegetation and anthropogenic features (e.g., buildings and industrial constructions) [55–58] and to obtain multiple DEMs at a 0.5 m spatial resolution (Figure 5).

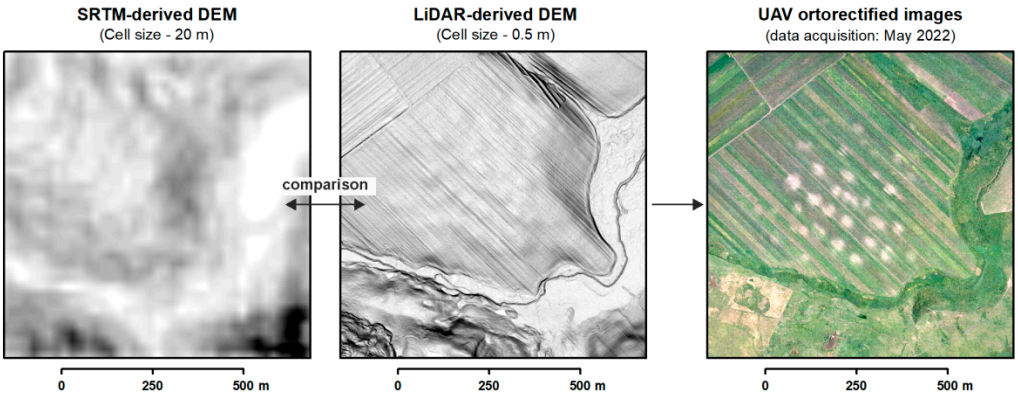

Figure 5. The difference between the SRTM-derived DEM with a 30 m cell size (left image) and the LiDAR-derived DEM with a 0.5 m cell size (middle image) generated for area of an NC-LBA site. The white spots visible on UAV orthorectified images (right image) indicate the ashmounds' pattern.

To simplify the GIS-based DEM data processing, a 500 m buffer area was computed around the centroid of each NC site to extract individual DEMs. The outcomes indicate high-quality DEMs of the bare ground because the data were acquired during the February–March period when the study area had low vegetation cover [31,53]. However, for the cases where the algorithm for point cloud classification failed (e.g., forests and built-up areas), which did not allow for the computation of geomorphological parameters (e.g., hypsometry, slopes, and the topographic position index) and the identification of visible ashmound structures on the settlement's surface, the final DEM was corrected and resampled at the same resolution.

3.3. Oblique and Vertical Aerial Photography

In order to determine the surface geomorphometric features of the ashmound structures inside the NC settlements, we created a geodatabase by using Google Earth Pro 7.1.5 and exported it as a shapefile in ArcGIS Pro. To validate the site locations of all 21 case studies, we used cartographic and aerial image products, including archaeological maps; topographic maps; orthophotos from Inis Viewer and Atlas Explorer portals; the high-resolution DEMs described in the section above [53]; and most importantly, the aerial images collected during fieldwork. We also compiled an inventory of sites by consulting the archaeological monographs for the Iași County [7,46,47]. During field surveys, we used unmanned aerial vehicle (UAV) technology [59–61] and managed to identify 200 visible ashmound structures (Figure 2). We captured aerial photographs by using a Phantom 4 Pro v.2 drone, acquiring oblique and vertical photographs with a minimum of 60% overlap between each photo. The flight altitude ranged between 50 and 75 m, and the photos were imported into Agisoft Metashape in order to obtain large orthorectified images (Figure 4) [60].

3.4. Morphometric Indices Computation

The basic processing of the aerial image was conducted by using ArcGIS Pro software, and the delineation of the ashmound features occurred through the on-screen digitization of the resulting orthophotos. The ground-point data obtained from the ALS survey were used to generate high-density LiDAR-derived DEMs [36] in the area of the selected NC-LBA sites. To obtain efficient results for the microlevel characterization of the ashmounds, the LiDAR-derived DEM with a resolution of 0.5 m was selected.

Geomorphometric properties are crucial indicators for surface processes, aiding in identifying the geomorphologic and surface-erosion aspects that affect archaeological structures such as the ashmound features. Therefore, various shape indices, including the area (A), perimeter (P), length (L), and others, were computed by using the *Calculated Geometry* tool in ArcGIS Pro software to perform a quantitative analysis of the ashmound

shape. In addition, several parameters for individual aspects, such as the form factor (RF) (Equation (1)), circularity ratio (RC) (Equation (2)), and elongation ratio (RE) (Equation (3)), were also calculated [62,63]:

$$RF = \frac{A}{L^2} \quad (1)$$

$$RC = \frac{12.57 \cdot A}{P^2} \quad (2)$$

$$RE = \frac{1.128\sqrt{A}}{L} \quad (3)$$

where A is the visible surface area (m^2), L is the ashmound maximum length (m), and P is the ashmound perimeter (m).

By analyzing the shape parameters, it was possible to gain a deeper understanding of the evolution of the ashmound morphometric characteristics, aiding in their identification and classification, due to the fact that:

- The RF reflects the ashmound's shape complexity;
- The RC helps determine the feature's degree of circularity;
- The RE provides information on the ashmound's length-to-breadth ratio, indicating the degree of elongation.

Therefore, by calculating and analyzing all three parameters, it was possible to obtain valuable information on the ashmound structure evolution.

Another morphometric parameter taken into consideration was the slope (S) of the visible ashmound surface. This is because the slope has a profound effect on both the water erosion potential and local wind systems, indicating the upper layers' displacement processes. In this study, the average values of the S parameter were computed also in ArcGIS software. However, for specialists who want to replicate these measurements but are not familiar with GIS-based measurements, the S parameter can be calculated by using Equation (4) [62,63]:

$$S = \frac{H_{max} - H_{min}}{L} \quad (4)$$

where H_{max} is the maximum elevation (m), H_{min} is the minimum elevation of the ashmound surface, and L is the ashmound's maximum length (m).

The last computed parameter was the hypsometric indices (HI). The HI of a surface like an ashmound is used to estimate the links between the horizontal area and its elevation. Currently, hypsometric curves are generated through GIS and have been widely used for the characterization of the landforms' evolution stage. In this study, the HI were calculated based on Equation (5) [62]:

$$HI = (H_{mean} - H_{min}) / (H_{max} - H_{min}) \quad (5)$$

where H_{mean} is the weighted mean elevation, H_{max} is the maximum elevation, and H_{min} is the minimum elevation of the ashmound surface.

4. Results and Discussion

4.1. Morphometric Description of the Selected Ashmound Structures

The descriptive statistics for the area (A), perimeter (P), and maximum length (L) parameters of the 200 ashmound features selected from the 21 NC archaeological sites are presented in Table 2. Additionally, Table 3 provides the descriptive statistics for the form factor (RF), circularity ratio (RC), and elongation ratio (RE).

Table 2. Descriptive statistics concerning area (A), perimeter (P), and maximum length (L) of the 200 ashmound features from the 21 NC archaeological sites (see Figure 1) from NE Romania (see Table S1).

Site Id	Number of Ashmounds	Area (m^2)				Perimeter (m)				Length (m)			
		Min	Med	Max	SD	Min	Med	Max	SD	Min	Med	Max	SD
S1	16	445.9	937.5	1847.7	±356.1	78.62	111.3	160.46	±20.19	29.34	40.27	59.23	±7.32
S2	10	764.8	1119.8	1519.7	±225.4	101.3	122.99	140.94	±13.55	31.9	43.55	54.44	±7.04
S3	2	497.5	799.4	1101.4	±302	81.37	100.31	119.25	±18.94	27.61	33.48	39.35	±5.87
S4	16	469.5	990.2	2224.4	±434.3	79.4	113.39	171.89	±23.11	26.62	39.9	58.77	±8.28
S5	13	470.3	1257.6	2656.6	±684.1	79.54	126.7	187.72	±32.68	27.43	45.79	66.6	±11.6
S6	8	300.1	889.5	1332.3	±348.5	62.79	107.34	135.49	±23.83	20.69	37.79	50.8	±9.2
S7	6	407.4	947.8	1369.4	±291.1	74.88	112.83	139.82	±19.87	28.03	41.15	49.76	±7.44
S8	7	314.7	681.4	1033.7	±278.7	67.23	94.03	118.29	±20.58	23.38	33.13	41.99	±7.16
S9	5	272.8	608.7	851.3	±215.2	61.06	88.88	106.76	±16.95	21.8	31.58	39.34	±6.36
S10	11	533.2	980.3	1804.6	±329.4	88.71	113.93	153.8	±16.94	34.16	41.19	53.57	±5.45
S11	19	662.4	1042	1744.7	±269.8	94.8	117.85	157.04	±15.31	33.86	41.94	60.18	±6.54
S12	5	570.3	901.9	1032.5	±169.6	86.72	109.49	119.7	±11.73	30.65	38.86	42.87	±4.45
S13	13	567.3	916.2	1231.9	±189.6	86.47	110.17	127.03	±11.9	30.61	38.81	44.22	±4.24
S14	4	562.9	897.6	1067	±200.9	87.32	108.8	120.1	±12.85	31.35	38.37	43.33	±4.49
S15	10	191.5	550	1110.4	±242.9	51.93	85.64	121.13	±18.85	20.14	32.2	47.18	±7.57
S16	9	286.2	686.7	1674.5	±367.1	61.42	92.73	147.79	±21.72	21.41	32.11	49.75	±7.17
S17	10	504.1	879.6	1101.2	±179.8	84.02	107.7	119.71	±11.07	31.28	37.97	44.42	±3.87
S18	5	590.1	1087.7	1487.3	±289.5	89.98	119.08	139.36	±16.21	33.72	41.51	48.82	±5.06
S19	5	404.8	841.6	1511.1	±394	73.44	104.8	144.78	±24.84	24.71	37.41	53.14	±9.93
S20	16	335.5	765	1307.4	±287.4	66.31	99.38	130.16	±18.92	22.84	35.43	45.91	±7.14
S21	10	388.6	814.5	1584.8	±361.4	71.23	101.6	143.31	±22.17	24.03	35.81	47.63	±7.66
Total	**200**	**191.5**	**905.2**	**2656.6**	**±381.3**	**51.93**	**108.34**	**187.72**	**±22.37**	**20.14**	**38.55**	**66.6**	**±8.21**

Table 3. Descriptive statistics concerning areal aspects, such as form factor (RF), circularity ratio (RC), and elongation ratio (RE) of 200 ashmound features from the 21 NC-LBA archaeological sites (see Figure 1) from NE Romania (see Table S1).

Site Id	Number of Ashmounds	Form Factor (RF)				Circularity Ratio (RC)				Elongation Ratio (RE)			
		Min	Med	Max	SD	Min	Med	Max	SD	Min	Med	Max	SD
S1	16	0.41	0.56	0.66	±0.07	0.82	0.92	0.96	±0.04	0.72	0.84	0.92	±0.06
S2	10	0.44	0.6	0.75	±0.1	0.85	0.92	0.97	±0.04	0.75	0.88	0.98	±0.07
S3	2	0.65	0.68	0.71	±0.03	0.94	0.96	0.97	±0.02	0.91	0.93	0.95	±0.02
S4	16	0.39	0.6	0.68	±0.08	0.79	0.93	0.96	±0.04	0.7	0.87	0.93	±0.06
S5	13	0.45	0.57	0.7	±0.08	0.85	0.92	0.98	±0.03	0.75	0.85	0.94	±0.06
S6	8	0.5	0.61	0.77	±0.08	0.9	0.93	0.96	±0.02	0.8	0.88	0.99	±0.06
S7	6	0.47	0.55	0.67	±0.06	0.88	0.91	0.96	±0.02	0.78	0.84	0.93	±0.05
S8	7	0.5	0.59	0.7	±0.06	0.88	0.93	0.95	±0.02	0.8	0.87	0.95	±0.04
S9	5	0.54	0.59	0.7	±0.06	0.92	0.93	0.97	±0.02	0.83	0.87	0.94	±0.04
S10	11	0.46	0.56	0.63	±0.06	0.85	0.92	0.96	±0.03	0.76	0.84	0.89	±0.05
S11	19	0.47	0.59	0.67	±0.06	0.87	0.93	0.96	±0.02	0.77	0.87	0.93	±0.05
S12	5	0.52	0.6	0.67	±0.05	0.91	0.94	0.96	±0.02	0.81	0.87	0.92	±0.04
S13	13	0.48	0.6	0.65	±0.04	0.89	0.94	0.96	±0.02	0.78	0.88	0.91	±0.03
S14	4	0.57	0.6	0.64	±0.03	0.93	0.94	0.95	±0.01	0.85	0.87	0.90	±0.02
S15	10	0.37	0.52	0.61	±0.07	0.82	0.9	0.95	±0.04	0.68	0.81	0.88	±0.06
S16	9	0.51	0.63	0.69	±0.06	0.88	0.95	0.97	±0.03	0.81	0.89	0.94	±0.04
S17	10	0.51	0.61	0.68	±0.07	0.9	0.94	0.97	±0.02	0.8	0.88	0.93	±0.05
S18	5	0.52	0.62	0.69	±0.06	0.92	0.94	0.96	±0.01	0.81	0.88	0.94	±0.05
S19	5	0.51	0.58	0.66	±0.06	0.85	0.91	0.96	±0.04	0.81	0.86	0.92	±0.04
S20	16	0.43	0.6	0.75	±0.09	0.84	0.94	0.98	±0.04	0.74	0.87	0.98	±0.07
S21	10	0.52	0.61	0.73	±0.07	0.91	0.95	0.97	±0.02	0.81	0.88	0.96	±0.05
Total	**200**	**0.37**	**0.59**	**0.77**	**±0.08**	**0.79**	**0.93**	**0.98**	**±0.03**	**0.68**	**0.86**	**0.99**	**±0.06**

The area of the visible ashmound structures ranges between 191.5 m^2 and 2656.6 m^2, with an average of 905.2 m^2 by taking into consideration all the selected features. The NC archaeological sites in which the average value is higher than 1000 m^2 are S2 (1119.8 m^2), S5 (1257.6 m^2), and S18 (1087.7 m^2), this being a consequence of their placement on the top of the hills, meaning they are affected by agricultural activity (a high erosion intensity). The archaeological sites with low average values for the visible ashmound areas include S8 (681.4 m^2), S9 (608.7 m^2), S15 (505 m^2), and S16 (686.7 m^2). In these sites, smaller

ashmounds are combined with one or two larger ashmound structures (e.g., S16, minimum area: 286.2 m^2; maximum area: 1674.5 m^2). However, a significant variation in the areas of the ashmound structures was identified across all of the selected NC archaeological sites (total SD: ±381.3 m^2; S12 minimum SD: ±169.6; S5 maximum SD: ±684.1). This variation can be explained by two factors. First, within each NC settlement with ashmounds, the intrasite area was severely affected by erosional or anthropogenic activities, leading to the destruction of the upper settlement layers and leaving behind only the ashmound basins (see Figure 2, Stage 5). This suggests that the ashmound structures had different surface areas initially. Second, within each site, the intrasite area was partially affected, and the ashmound structures are visible in different stages of erosion (see Figure 2, Stage 2 to 4). This indicates that the ashmound structures initially had similar areas. However, we believe that the first scenario provides a better explanation for the initial dimensions of these structures. This is supported by the fact that the area of the largest visible ashmound structure (2656.6 m^2) is 13.8 times larger than the area of the smallest structure identified (191.5 m^2) (Table 2).

Generally, the perimeter (P) is strongly correlated with the area (A) and length (L) of the irregular surfaces. In the case of the visible ashmound structures, the P parameter ranges from 51.93 m to 187.72 m, with an average value of 108.34 m. Among the archaeological sites in question, S2 (122.99 m), S5 (126.7 m), and S18 (119.08 m) have higher average perimeter (P) values compared to the other sites, similar to the trend observed for the area (A) parameter. However, as the perimeter (P) increases, the length (L) also tends to increase, given that the smoothness of the ashmound structure's margins is low. Consequently, the maximum length (L) of the investigated archaeological structures varies from 20.14 m to 66.6 m, with an average value of 38.55 m. The NC sites that present higher average length (L) values (>40 m) of the ashmound structures are: S2 (43.55 m), S5 (45.79 m), S7 (41.15 m), S10 (41.19 m), S11 (41.94 m), and S18 (41.51 m) (Table 2). This variation in the L parameter can be explained in certain cases (e.g., S7) by mechanized agricultural activities that have disrupted the top layer of the ashmound structures, stretching the accumulated material along the plowing direction. This aspect transformed the surface of the investigated archaeological structures, in most cases, from a circular shape, believed to be their initial form, into an ellipsoid with a longer axis aligned with the agricultural operations.

However, for a better understanding of the evolution of the ashmound's morphometric characteristics based on the area (A), perimeter (P), and maximum length (L) parameters, we calculated the form factor (RF), circularity ratio (RC), and elongation ratio (RE). The descriptive statistics concerning areal aspects based on these parameters are indicated in Table 3.

The first surface aspect parameter used to characterize the visible ashmound is the form factor (RF), which has been selected for this approach because it reflects the shape complexity of the investigated archaeological structures. In this context, the RF is defined as the ratio of the ashmound area (A) to the square of its length (L). Low RF values (<0.5) indicate long and narrow forms of the visible archaeological structures, while high RF values (>0.5) indicate a more circular shape. In the study area, the RF of the visible ashmounds' surface ranges between 0.37 and 0.77, with an average of 0.59 across all 200 investigated features. Furthermore, more than 85% of the selected ashmound structures (174 ashmounds) exhibit a more circular shape, while only 13% of them have an elongation index (RF) less than 0.5. This suggests that 26 of the analyzed archaeological structures have been severely impacted by anthropogenic activities (Table 3).

The circularity ratio (RC), which is defined as the ratio of the basin area to the area of a circle with the same perimeter as the drainage basin, was the second surface aspect parameter used to characterize the ashmound features. Similar to the RF, a low value of the RC indicates a complex and sinuous form, while a value close to one indicates a circular shape. For the analyzed archaeological structures, the RC ranges between 0.79 and 0.98, with an average of 0.93, out of which 175 ashmound structures indicate a circularity ratio

value more than 0.9. What stands out in the values of the RC parameter is that all the ashmound features exhibit a form based on circles, with values close to one indicating that those structures have reached the stage of advanced degradation when only the ashmound basin remains (see Figure 2; Table 3).

The last surface ratio parameter considered for the ashmound surface characterization was the elongation ratio (RE). The RE is defined as the ratio of the diameter of a circle with the same area as the visible ashmound structure to the maximum length of the ashmound. In the case of the studied features, the RE ranges between 0.68 and 0.99, with an average of 0.86. A low RE value (<0.75) indicates ashmounds with steep slopes that are sensitive to erosion. In this particular case, eight ashmound structures within the S1, S2, S4, S12, S15, S16, and S20 NC archaeological sites exhibit high sensitivity to erosion due to the predominantly steep slope surface (Table 3). However, a more detailed analysis of the implications of the slope and elevation for the ashmound structure characterization will be provided below, focusing on the computation of the relief aspects such as the hypsometric indices (HI) (Table 4).

Table 4. Descriptive statistics concerning terrain slope (S) and relief aspects computed based on hypsometric indices (HI) of 200 ashmound features from the 21 NC-LBA archaeological sites (see Figure 1) from NE Romania (see Table S1).

Site Id	Number of Ashmounds	Slope (°)				HI			
		Min	Med	Max	SD	Min	Med	Max	SD
S1	16	0.23	4.93	12.38	±2.12	0.45	0.5	0.55	±0.02
S2	10	0.4	4.17	8.47	±1.30	0.45	0.49	0.53	±0.02
S3	2	0.03	0.58	1.43	±0.27	0.57	0.58	0.59	±0.01
S4	16	0.57	3.92	7.49	±1.12	0.43	0.53	0.58	±0.04
S5	13	0.69	5.26	11.16	±1.66	0.42	0.49	0.56	±0.04
S6	8	1.88	5.64	7.93	±0.98	0.49	0.5	0.52	±0.01
S7	6	0.69	4.70	8.47	±1.34	0.47	0.53	0.58	±0.03
S8	7	0.36	4.53	12.16	±2.16	0.43	0.49	0.57	±0.05
S9	5	1.17	5.15	9.40	±1.52	0.48	0.53	0.59	±0.04
S10	11	0.22	3.52	7.74	±1.28	0.44	0.52	0.57	±0.04
S11	19	0.57	4.59	9.06	±1.38	0.45	0.48	0.51	±0.02
S12	5	0.36	5.91	14.28	±2.48	0.44	0.48	0.51	±0.03
S13	13	0.87	5.58	10.41	±1.68	0.44	0.5	0.57	±0.03
S14	4	0.2	4.40	12.11	±2.08	0.44	0.51	0.54	±0.04
S15	10	0.79	5.11	10.82	±1.70	0.35	0.5	0.58	±0.06
S16	9	0.64	2.98	4.63	±0.87	0.42	0.5	0.58	±0.04
S17	10	0.43	6.26	13.64	±2.17	0.44	0.48	0.51	±0.02
S18	5	0.09	6.33	19.69	±3.35	0.46	0.49	0.51	±0.02
S19	5	0.06	2.80	7.26	±1.41	0.34	0.47	0.58	±0.1
S20	16	1.11	6.65	12.12	±1.76	0.43	0.49	0.55	±0.03
S21	10	0.33	3.14	7.12	±1.22	0.49	0.53	0.61	±0.04
Total	**200**	**1.11**	**4.58**	**19.69**	**±1.61**	**0.34**	**0.50**	**0.61**	**±0.04**

As mentioned earlier, only two relief aspects were computed for the surface characterization of ashmound structures, namely the slope (S) and hypsometric indices (HI). We selected these indices for their ability to describe the micromorphology of the studied archaeological features by using LiDAR-derived DEMs. Additionally, these indices have the predictive capability to indicate processes of upper layer displacement within NC settlements. Therefore, the average values of the terrain slope (S) on the surface of the ashmound structures range between 1.17° and 19.69°, with an average of 4.58°. Among the sites in question, S1, S8, S12, S14, S17, S18, and S20 exhibit maximum values (>15°) of the slope parameter. These terrain slope characteristics are a consequence of the placement of NC sites in areas affected by anthropogenic erosion, such as arable land, and other degradation processes, including gully erosion in the case of S18 (S max. 19.69°) (Table 4). Furthermore, the slope parameter (S) also indicates the characteristics of habitation practices and the preferred landform types for NC communities. In this regard, all of the investigated sites were located on open slopes, near stream confluences with relatively well-developed

floodplains, or in the close proximity of hilltops. However, for more information on the connection between the NC habitation practices and the slope types, please refer to our previous publication [7].

Regarding the hypsometric indices (HI), this relief parameter is useful in explaining the erosion that has occurred as a result of hydromorphological processes and the variables contributing to land degradation in the investigated area. Regarding the surface of the analyzed ashmound structures, the results indicate that 112 ashmounds still exhibit convex landforms in the landscape (HI > 0.5), 26 ashmound structures have a flat surface (HI = 0.5), and only 62 ashmound structures are currently in concave landforms (HI < 0.5). Regarding the sites, the average value of the HI parameter indicates that nine sites have slightly concave ashmound surfaces, five sites have flat ashmounds, and the remaining seven sites still have ashmounds with slightly convex surfaces (Table 4). However, based on the slope (S) conditions and the hypsometric indices (HI) calculated from the ashmounds' surfaces, it is clear that all the analyzed ashmound structures are in either the first erosion phase, affecting both the older soil layer and the ashmound structure (Figure 2, Stage 4), or in the second erosion phase, where the destruction of the upper settlement layers is almost complete, with the ashmound basin being the only one still left (Figure 2, Stage 5).

4.2. Trends in Ashmound Structures' Evolutionary Pattern

Regarding the trend evolution of the visible surfaces of the ashmound structures, and consequently their associated basins, it has been noticed that the temporal dynamics are consistent with those described by Dietrich [9] (see Figure 2). Thus, based on the values of the RF, RC, and RE indices, all 200 surfaces attributed to the NC ashmound structures analyzed in this study indicate that they are in the first (Stage 4) or second (Stage 5) erosion phase, where the destruction of the upper settlement layers is almost complete and only the ashmound basin remains. However, in a previous study [7], based on the assumption that there is a correlation between the visible surface and the degree of the preservation of the ashmounds basin, i.e., the smaller the visible surface, the deeper the structure, this assumption was contradicted by archaeological excavations.

Therefore, by analyzing the length–area dataset as a function of the surface shape, the trend of the three computed shape indices indicates that the shape ratio, circularity, or elongation are not influenced by the size (area and perimeter) or maximum length of the visible surfaces of the ashmounds, only by their degree of degradation. Thus, as a top layer structure becomes more eroded, the values of the RF, RC, and RE deviate from the initial circular shape until the topographic surface coincides with the surface of the initial basin (Figure 6, left charts). In this regard, the RF values for the 200 investigated ashmound structures indicate a slight tendency of waviness in the visible boundaries due to repeated anthropogenic interventions. In the case of the RC, the values indicate a high level of preservation of the initial circular form, mainly because the initial level of the structures has been removed, leaving only the visible form of the initial basin. As for the RE values, they indicate the elongation of the surfaces only in the case of the structures in Stage 4 of degradation according to [9], as in these situations, the circular boundaries of the ashmound basin are not yet visible (Figure 6, right charts).

The same trend of evolution, as observed in the case of the shape indices, is also evident from the analysis of the values of the hypsometric indices (HI) computed for the visible surfaces of the ashmound structures. Therefore, the values of the HI parameters indicate that the initial landform aspect of the ashmound structure, assumed to be convex compared to the topographic surface during the LBA period, has been almost completely removed. This flattening trend, present in all the analyzed structures, also does not correlate with any other shape parameter of the visible ashmound structures, which reinforces the idea that the initial size of the basins varied in area (A), perimeter (p), and maximum length (L) (Figure 7, left chart). Therefore, the relief aspect from the present time cannot indicate the initial height of the mixture of terrigenous and archaeological materials deposited

in these basins, only their degree of deterioration in relation to erosional processes and anthropogenic activities that have modified their specific landform (Figure 7, right chart).

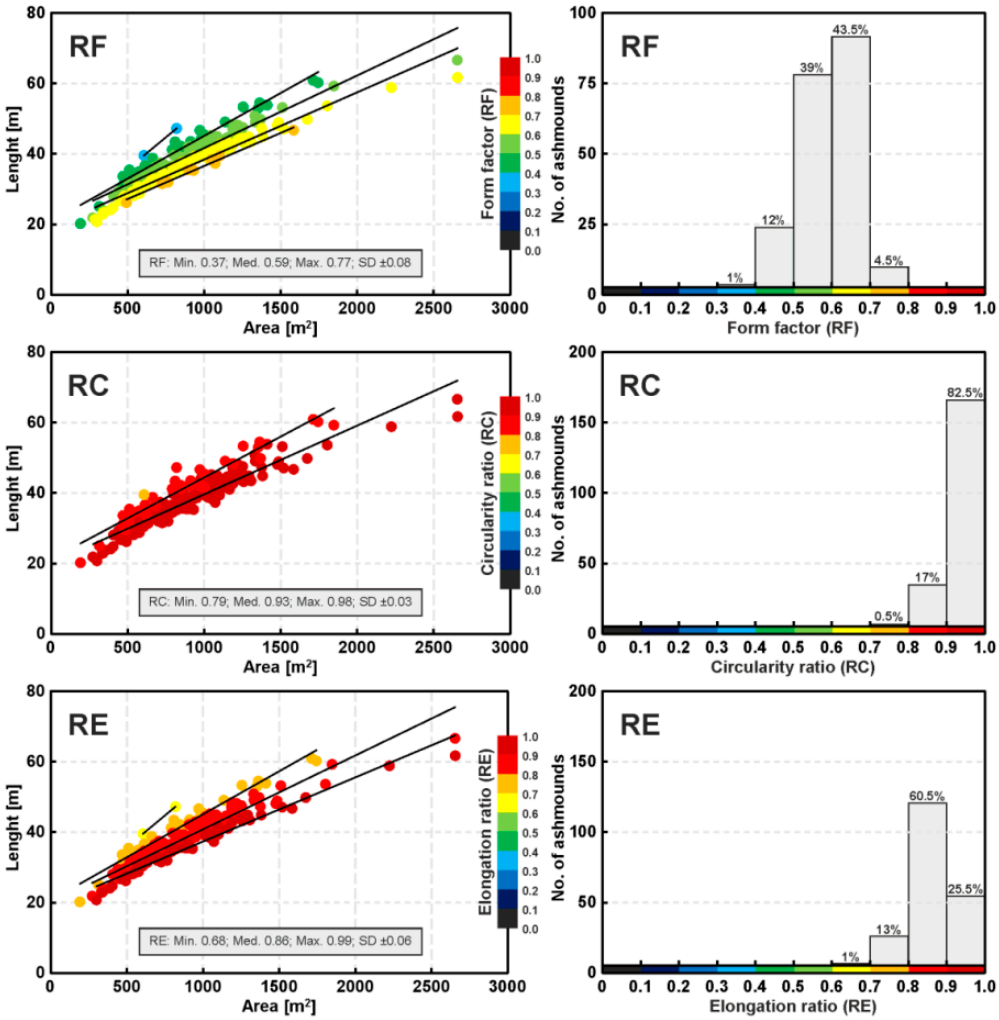

Figure 6. Length–area dataset from 200 ashmound features from NE Romania as a function of surface shape (**left charts**). Color code is for the form factor (RF), circularity ratio (RC), and elongation ratio (RE). Black lines represent the best fit obtained for subsets based on class intervals. The number of ashmound features for each class of RF, RC, and RE (**right charts**) and its associated proportion within the dataset.

4.3. Limitation of the GIS-Based Ashmound Features Characterization

Like any investigation involving the use of Airborne Laser Scanning (ALS) and aerial photography (AP) techniques, as well as the processing of the resulting spatial data in GIS, the methodology used in this study has certain limitations. Firstly, the collection of aerial photogrammetric data, acquired in order to identify soil marks associated with the NC ashmounds, is dependent on the vegetation season. Under these conditions, the best images were captured only during fresh plowing, specifically in the spring season, which limits survey campaigns to a few months each year. Additionally, in areas with different vegetation patches, direct ground measurements are required in agricultural parcels where the ashmound pattern is obscured. Furthermore, these measurements involve expert opinions, such as geomorphologists, pedologists, and archaeologists, to confirm changes in the soil texture and archaeological content in the area where the boundaries of these archaeological structures are lost under vegetation.

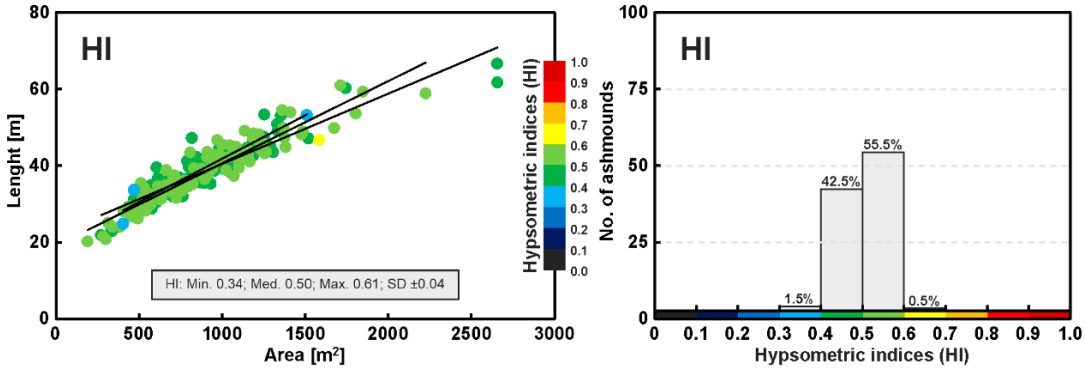

Figure 7. Length–area dataset of 200 ashmound features from NE Romania as a function of surface shape (**left charts**). Color code is for the hypsometric indices (HI). Black lines represent the best fit obtained for subsets based on class intervals. The number of ashmound features for each class of HI (**right charts**) and its associated proportion within the dataset.

Furthermore, the GIS analysis of the ashmound microstructures depends on the availability of highly accurate DEMs, such as LiDAR-derived DEMs, and involves processing a large database. Even under these conditions, high-resolution terrain elevation models bring significant changes from year to year at the ground level due to agricultural activities that can reach depths of 40–50 cm and substantially alter the morphometric and morphological parameters of the ashmounds. For this reason, in this study, in order to characterize the visible surface of the ashmounds, we calculated only those shape (area, perimeter, maximum length, form factor, circularity ratio, and elongation ratio) and relief (terrain slope and hypsometric indices) parameters that are not directly dependent on the raster resolution. Nevertheless, the surface analysis of the archaeological structures in question provides valuable information for studying the LBA period and opens up a new research direction regarding the micromorphometry of the NC settlements with ashmounds. Our next objective will be correlating the information obtained in this study with data related to the depth and internal structure of the ashmounds.

5. Conclusions

The GIS-based surface characterization of 200 ashmound structures with temporal resolution, identified by using Airborne Laser Scanning (ALS) and aerial photography (AP) techniques, for 21 NC archaeological sites provides valuable morphometric information related to cultural heritage remains from northeastern Romania. Within this framework, by computing six shape parameters including the area (A), perimeter (P), length (L), form factor (RF), circularity ratio (RC), and elongation ratio (RE), along with two relief aspects, the slope (S) and hypsometric indices (HI), specifically for the selected ashmound structures, the following main conclusions can be drawn:

- Based on the shape parameters, the area (A) of the visible ashmound structures ranges from 191.5 m^2 to 2656.6 m^2, with an average of 905.2 m^2. The perimeter (P) of these structures ranges from 51.93 m to 187.72 m, with an average value of 108.34 m. Furthermore, the maximum length (L) of the investigated archaeological structures varies from 20.14 m to 66.6 m, with an average value of 38.55 m. The variation in the values of the A, P, and L parameters can be attributed to anthropogenic activities, such as mechanized agriculture, which have disturbed the top layer of the ashmound structures and caused the material to stretch along the plowing direction.
- Based on the computed shape indices, the form factor (RF) of the visible ashmound surfaces ranges from 0.37 to 0.77, with an average of 0.59. The circularity ratio (RC) ranges from 0.79 to 0.98, with an average of 0.93. Notably, 175 ashmound structures exhibit circularity ratio values higher than 0.9. Additionally, the elongation ratio (RE) ranges from 0.68 to 0.99, with an average of 0.86. The values of the RF, RC, and RE consistently indicate a transformation process of the visible ashmound surfaces. In most

cases, the original circular shape, believed to be the initial form of the ashmounds, has been altered into an ellipsoid with a longer axis aligned with agricultural operations.

- Based on the relief aspects of the visible ashmound structures, the computed values for the terrain slope (S) range from 1.17° to 19.69°, with an average of 4.58° for each investigated archaeological structure. In terms of the hypsometric indices (HI), the results indicate that 112 ashmounds still maintain convex landforms in the landscape (HI > 0.5), 26 ashmound structures have a flat surface (HI = 0.5), and only 62 ashmound structures currently exhibit concave landforms (HI < 0.5). Overall, considering the relief aspects, it can be concluded that all the analyzed ashmound structures are either in the first erosion phase, affecting both the older soil layer and the ashmound structure, or in the second erosion phase, where the destruction of the upper settlement layers is nearly complete, leaving only the ashmound basin intact. Thus, the analysis carried out in the present study has been able to demonstrate that, out of the few models of ashmound formation stated so far [9,16,18], the closest to reality is the one formulated by L. Dietrich, according to which the ashmounds, as we know nowadays, have been subjected to various transformations that can be synthetized in five stages: first, an oval basin was dug up from the LBA stepping level; next, the basin starts to slowly fill up, while on the LBA ground surface, the cultural layer starts to build up; the third stage is represented by the abandonment of the settlements, and it corresponds to the maximum height of the ashmound; the next two phases are the ones addressed in the current paper, and they include the ulterior anthropic activities that flatten the surface of the ashmound, until it no longer presents any elevation, as evidenced by the analysis performed on the various shape and surface characteristics of 200 such features.

From the perspective of the combined ALS, AP, and GIS methodology applied in this study, even though it has several limitations in terms of characterizing archaeological structures with temporal resolution, we believe that it represents a valuable tool for comprehending the habitation patterns and ecocultural evolution of prehistoric communities belonging to the NC. Therefore, we intend to correlate the information obtained in this study with data pertaining to the depth and internal structure of the ashmounds in future research endeavors.

Supplementary Materials: The following supporting information can be downloaded at https://www.mdpi.com/article/10.3390/rs15174124/s1: Table S1: Name, location, and morphometric parameters of 200 visible ashmound structures specific to 21 NC-LBA sites in NE Romania.

Author Contributions: Conceptualization, C.B. and A.M.-P.; methodology, C.B., A.M.-P. and R.-A.B.; software, C.B., A.M.-P. and R.-A.B.; validation, C.B. and A.M.-P.; formal analysis, C.B., A.M.-P. and R.-A.B.; investigation, C.B., A.M.-P. and R.-A.B.; resources, C.B.; data curation, C.B. and A.M.-P.; writing—original draft preparation, C.B., A.M.-P. and R.-A.B.; writing—review and editing, C.B. and A.M.-P.; visualization, C.B., A.M.-P. and R.-A.B.; supervision, C.B. and A.M.-P.; project administration, C.B.; funding acquisition, C.B. All authors have read and agreed to the published version of the manuscript.

Funding: Authors are thankful to Romanian Ministry of Research, Innovation and Digitization, within Program 1—Development of the national RD system, Subprogram 1.2—Institutional Performance—RDI excellence funding projects, Contract no.11PFE/30.12.2021, for financial support.

Data Availability Statement: The data presented in this study are contained within the article and supplementary material.

Acknowledgments: LiDAR data were provided by NARW-PBWA based on the institutional collaboration protocol between PBWA and ICI-UAIC. We thank two anonymous reviewers whose comments helped improve and clarify this manuscript.

Conflicts of Interest: The authors declare no conflict of interest. The founding sponsors had no role in the design of the study; in the collection, analyses, or interpretation of data; in the writing of the manuscript; or in the decision to publish the results.

Abbreviations

The following abbreviations are used in this manuscript:

A	Area
ALS	Airborne Laser Scanning
BA	Bronze Age
BP	Before Present
DEM	Digital Elevation Model
GIS	Geographic Information System
H	Elevation
HI	Hypsometric Indices
IA	Iron Age
L	Maximum length
LBA	Late Bronze Age
LiDAR	Light Detection and Ranging
MBA	Middle Bronze Age
NARW-PBWA	Romanian Waters—Prut–Bîrlad Water Administration
NC	Noua Culture
NSC	Noua-Sabatinovka-Coslogeni
P	Perimeter
PBRB	Prut–Bîrlad River Basin
RC	Circularity ratio
RE	Elongation ratio
RF	Form factor
RS	Remote sensing
S	Terrain slope
S1-S21	NC-LBA sites
SD	Standard Deviation
SRTM	Shuttle Radar Topography Mission
UAV	Unmanned aerial vehicle

References

1. Feurdean, A.; Klotz, S.; Mosbrugger, V.; Wohlfarth, B. Pollen-based quantitative reconstructions of Holocene climate variability in NW Romania. *Paleogeogr. Paleoclimatol. Paleoecol.* **2008**, *260*, 494–504.
2. Harding, A.F. *European Societies in the Bronze Age*; Cambridge University Press: Cambridge, UK; New York, NY, USA, 2000.
3. Wittenberger, M. Economical life in Noua Culture in the Transylvanian Late Bronze Age. *Acta Musei Napoc.* **2008**, *43–44*, 5–46.
4. Petrescu-Dîmbovița, M. Perioada târzie a Epocii Bronzului. In *Istoria Românilor*, 2nd ed.; Petrescu-Dîmbovița, M., Vulpe, A., Eds.; Editura Enciclopedică: București, Romania, 2010; pp. 266–281.
5. Florescu, A.C. Contribuții la cunoașterea culturii Noua. *Arheol. Mold.* **1964**, *II–III*, 143–216.
6. Petrescu-Dîmbovița, M. Perioada târzie a Epocii Bronzului. In *Istoria Românilor*, 1st ed.; Petrescu-Dîmbovița, M., Vulpe, A., Eds.; Editura Enciclopedică: București, Romania, 2010; pp. 272–287.
7. Mihu-Pintilie, A.; Brașoveanu, C.; Stoleriu, C.C. Using UAV Survey, High-Density LiDAR Data and Automated Relief Analysis for Habitation Practices Characterization during the Late Bronze Age in NE Romania. *Remote Sens.* **2022**, *14*, 2466. [CrossRef]
8. Sava, E. Die spätbronzezeitlichen Aschehügel („Zol'niki")-ein Erklärungsmodell und einige historisch-wirtschaftliche Aspekte. *Prähistorische Z.* **2005**, *80*, 65–109.
9. Dietrich, L. Visible workshops for invisible commodities. Leatherworking in the Late Bronze Age Noua culture's ‚ashmounds'. In *Din Preistoria Dunării de Jos. 50 de ani de la Începutul Cercetărilor Arheologice la Babadag (1962–2012)*; Ailincăi, S.C., Țârlea, A., Micu, C., Eds.; Editura Istros: Brăila, Romania, 2013; pp. 227–246.
10. Dietrich, L. Purity and holy dumps of garbage: Organising rubbish disposal in the Middle and Late Bronze Age of the Carpathian Basin. In *Archaeologies of Waste. Encounters with the Unwanted*; Sosna, D., Brunclíková, L., Eds.; Oxbow Books: Oxford, UK, 2017; pp. 23–40.
11. Zaretskyi, I.A. Za-metka o drevnostyakh Khar'kovskoy gub. In *Bogodukhovskogo Uyezda, Slobody Likha-Chevki*; Khar'kovskiy sbornik: Kharkiv, Ukraine, 1888.
12. Gorodčov, V.A. Dnevnik arkheologicheskikh issledovaniy v Zen'kovskom uyezde Poltavskoy gubernii v 1906 g. Issledovaniye Bel'skogo gorodishcha. In *Trudy 14 Arkheologi-Cheskogo s"yezda v Chernigove*; Moskva, Russia, 1911; Volume 3, pp. 93–161.
13. Sava, E. *Așezări din Perioada Târzie a Epocii Bronzului în Spațiul Pruto-Nistrean (Noua-Sabatinovka)*; Bons Offices: Chișinău, Republic of Moldova, 2014.
14. Petrescu-Dîmbovița, M. Contribuții la problema sfîrșitului epocii bronzului și începutului epocii fierului în Moldova. *Stud. Cercet. Istor. Veche Arheol.* **1953**, *IV*, 3–25.

15. Terenožkin, A.I. *Predskifskiy period na Dneprov-skom Pravoberezh'ye (Pre-Scythian period on the Dnieper Right Bank)*; Izd-vo Akademii nauk Ukr. SSR: Kiyev, Ukraine, 1961.
16. Gershkovich, J.P. Farmers and Pastoralists of the Pontic Lowland during the Bronze Age. In *Prehistoric Steppe Adaptation and the Horse*; Levine, M., Renfrew, C., Boyle, K., Eds.; McDonald Institute for Archaeological Research: Cambridge, UK, 2003; pp. 307–318.
17. Dobrinescu, C.; Haită, C. Așezări de tip cenușar din bronzul târziu în Sud-Estul României. *Cult. Civilizație Dunărea Jos* **2005**, *XXII*, 421–428.
18. Sava, E.; Kaiser, E. *Poselenie s „zolnicami" u acela Odaia-Miciurin, Respublica Moldova (Arheologhicesne i Estestvennonaucinie Issledovaniia)/Die Siedlung mit „Aschenhügeln" beim Dorf Odaia-Miciurin, Republik Moldova (Archäologische und Naturwissenschaftliche Untersuchungen)*; Bons Offices: Chișinău, Republic of Moldova, 2011.
19. Kaiser, E.; Sava, E.; Sîrbu, M.; Mistreanu, E.; Bubulici, V. Similar but Different! Late Bronze Age Settlement Features in the Steppe and Forest Steppe. In *Objects, Ideas and Travelers. Contacts between the Balkans, the Aegean and Western Anatolia during the Bronze and Early Iron Age*; Maran, J., Băjenaru, R., Ailincăi, S.-C., Popescu, A.-D., Hansen, S., Eds.; Verlag Dr. Rudolf Habelt GmbH: Bonn, Germany, 2020; pp. 395–415.
20. Wilson, D.R. *Air Photo Interpretation for Archaeologists*; B.T. Batsford: London, UK, 1982.
21. Bewley, R.H. Aerial photography for archaeology. In *Archaeological Method and Theory: An Encyclopedia*; Ellis, L., Ed.; Garland Publishing: New York, NY, USA; London, UK, 2000; pp. 3–10.
22. Stular, B.; Kokalj, Z.; Ostir, K.; Nuninger, L. Visualization of LiDAR-derived relief models for detection of archaeological features. *J. Archaeol. Sci.* **2012**, *39*, 3354–3360. [CrossRef]
23. Ceraudo, G. Aerial Photography in Archaeology. In *Good Practice in Archaeological Diagnostics. Non-Invasive Survey of Complex Archaeological Sites*; Corsi, C., Slapšak, B., Vermeulen, F., Eds.; Springer: Cham, Switzerland, 2013; pp. 11–30.
24. Yokoyama, R.; Sirasawa, M.; Pike, R.J. Visualizing topography by openness: A new application of image processing to digital elevation models. *Photogramm. Eng. Remote Sens.* **2002**, *68*, 257–265.
25. Kokalj, Ž.; Zakšek, K.; Oštir, K. Visualization of LiDAR derived relief models. In *Interpreting Archaeological Topography: Airborne Laser Scanning, 3D Data and Ground Observation*; Opitz, R.S., Cowley, D., Eds.; Oxbow Books: Oxford, UK, 2013; Volume 5, pp. 100–114.
26. Chase, A.S.Z.; Chase, D.Z.; Chase, A.F. LiDAR for Archaeological Research and the study of Historical Landscapes. In *Sensing the Past: From Artifact to Historical Site*; Masini, N., Soldovieri, F., Eds.; Springer International Publishing: Cham, Switzerland, 2017; pp. 89–100.
27. Palmer, R. Implicații ale arheologiei aeriene pentru arheologia din România. In *Arheologie Aeriană în România și în Europa*; Palmer, R., Târnoveanu, I.O., Bem, C., Eds.; Institutul de Memorie Culturală (CIMEC): București, Romania, 2009; pp. 8–61.
28. Târnoveanu, I.O.; Bem, C. România: Un viitor pentru trecut. Fotografiile aeriene în repertorierea siturilor arheologice. In *Arheologie Aeriană în România și în Europa*; Palmer, R., Târnoveanu, I.O., Bem, C., Eds.; Institutul de Memorie Culturală (CIMEC): București, Romania, 2009; pp. 62–88.
29. Asăndulesei, A. GIS (Geographic Information System), fotogrametrie și geofizică în arheologie. In *Investigații Non-Invazive în Așezări Cucuteni din România*; Editura Universității „Alexandru Ioan Cuza" din Iași: Iași, Romania, 2015.
30. Asăndulesei, A. Inside a Cucuteni Settlement: Remote Sensing Techniques for Documenting an Unexplored Eneolithic Site from Northeastern Romania. *Remote Sens.* **2017**, *9*, 41.
31. Niculiță, M. Geomorphometric Methods for Burial Mound Recognition and Extraction from High-Resolution LiDAR DEMs. *Sensors* **2020**, *20*, 1192. [CrossRef]
32. Sîrbu, V.; Ștefan, M.-M.; Ștefan, D. *A Monumental Hellenistic Funerary Ensemble at Callatis on the Western Black Sea. The Documaci Tumulus*; Archaeopress Publishing: Oxford, UK, 2021; Volume 1.
33. Bicbaev, V.; Sava, E. Interpretarea fotografiilor aeriene ale unor situri Noua. *Mem. Antiq.* **2004**, *XXIII*, 335–353.
34. Brașoveanu, C. Perioada Târzie a Epocii Bronzului în Bazinul Jijiei (România). Habitat și materialitate. Ph.D. Thesis, Alexandru Ioan Cuza University of Iași, Iași, Romania, 2021.
35. Agapiou, A.; Hegyi, A.; Gogâltan, F.; Stavilă, A.; Sava, V.; Sarris, A.; Floca, C.; Dorogostaisky, L. Exploring the largest known Bronze Age earthworks in Europe through medium resolution multispectral satellite images. *Int. J. Appl. Earth Obs. Geoinf.* **2023**, *118*, 103239. [CrossRef]
36. Roberts, K.C.; Lindsay, J.B.; Berg, A.A. An Analysis of Ground-Point Classifiers for Terrestrial LiDAR. *Remote Sens.* **2019**, *11*, 1915. [CrossRef]
37. Stoleriu, C.C.; Urzica, A.; Mihu-Pintilie, A. Improving flood risk map accuracy using high-density LiDAR data and the HEC-RAS river analysis system: A case study from north-eastern Romania. *J. Flood Risk Manag.* **2020**, *13*, e12572. [CrossRef]
38. Romanescu, G.; Pascal, M.; Mihu-Pintilie, A.M.; Stoleriu, C.C.; Sandu, I.; Moisii, M. Water Quality Analysis in Wetlands Freshwater: Common Floodplain of Jijia-Prut Rivers. *Rev. Chim. (Buchar.)* **2017**, *68*, 553–561. [CrossRef]
39. Huţanu, E.; Mihu-Pintilie, A.; Urzica, A.; Paveluc, L.E.; Stoleriu, C.C.; Grozavu, A. Using 1D HEC-RAS Modeling and LiDAR Data to Improve Flood Hazard Maps Accuracy: A Case Study from Jijia Floodplain (NE Romania). *Water* **2020**, *12*, 1624. [CrossRef]
40. Mihu-Pintilie, A.; Nicu, I.C. GIS-based Landform Classification of Eneolithic Archaeological Sites in the Plateau-plain Transition Zone (NE Romania): Habitation Practices vs. Flood Hazard Perception. *Remote Sens.* **2019**, *11*, 915. [CrossRef]

41. Niculiță, M.; Mărgărint, M.C.; Santangelo, M. Archaeological evidence for Holocene landslide activity in the eastern Carpathian lowland. *Quat. Int.* **2016**, *415*, 175–189. [CrossRef]
42. Haase, D.; Fink, J.; Haase, G.; Ruske, R.; Pécsi, M.; Richter, H.; Altermann, M.; Jäger, K.-D. Loess in Europe—Its spatial distribution based on a European loess map, scale 1:250,000. *Quat. Sci. Rev.* **2007**, *26*, 1301–1312. [CrossRef]
43. Romanescu, G.; Cîmpianu, C.I.; Mihu-Pintilie, A.; Stoleriu, C.C. Historic flood events in NE Romania (post-1990). *J. Maps* **2017**, *13*, 787–798. [CrossRef]
44. Mihu-Pintilie, A.; Gherghel, I. Eco-cultural niche breadth and overlap within the Cucuteni–Trypillia Culture groups during the Eneolithic. *Front. Earth Sci.* **2022**, *10*, 910836. [CrossRef]
45. Dascălu, L. *Bronzul Mijlociu și Târziu în Câmpia Moldovei*; Editura Trinitas: Iași, Romania, 2007.
46. Chirica, V.; Tanasachi, M. *Repertoriul Arheologic al Județului Iași, Volume I*; Institutul de Istorie și Arheologie "A. D. Xenopol": Iași, Romania, 1984.
47. Chirica, V.; Tanasachi, M. *Repertoriul arheologic al județului Iași, Volume II*; Institutul de Istorie și Arheologie "A. D. Xenopol": Iași, Romania, 1985.
48. Păunescu, A.; Șadurschi, P.; Chirica, V. *Repertoriul Arheologic al Județului Botoșani*; Institutul de Arheologie București: București, Romania, 1976.
49. Șovan, O.L. *Repertoriul Arheologic al Județului Botoșani*, 2nd ed.; Editura Pim: Botoșani, Romania, 2016.
50. Vizireanu, I.; Mateescu, R. The Potential of Airborne LiDAR for Detection of New Archaeological Site in Romania. In *Diversity in Coastal Marine Sciences*; Finkl, C., Makowski, C., Eds.; Coastal Research Library; Springer: Cham, Switzerland, 2018; pp. 617–630.
51. Doneus, M. Openness as Visualization Technique for Interpretative Mapping of Airborne Lidar Derived Digital Terrain Models. *Remote Sens.* **2013**, *5*, 6427–6442. [CrossRef]
52. Garcia-Molsosa, A.; Orengo, H.A.; Lawrence, D.; Philip, G.; Hopper, K.; Petrie, C.A. Potential of deep learning segmentation for the extraction of archaeological features from historical map series. *Archaeol Prospect.* **2021**, *28*, 187–199. [CrossRef] [PubMed]
53. SMIS-CSNR 17945 (Water Administration Prut—Bîrlad, Romania) Works for Reducing the Flood Risk in Prut—Bîrlad Basin. Available online: http://www.romair.ro (accessed on 28 March 2023).
54. Mihu-Pintilie, A.; Cîmpianu, C.I.; Stoleriu, C.C.; Pérez, M.N.; Paveluc, L.E. Using High-Density LiDAR Data and 2D Streamflow Hydraulic Modeling to Improve Urban Flood Hazard Maps: A HEC-RAS Multi-Scenario Approach. *Water* **2019**, *11*, 1832. [CrossRef]
55. Zhang, W.; Qi, J.; Wan, P.; Wang, H.; Xie, D.; Wang, X.; Yan, G. An Easy-to-Use Airborne LiDAR Data Filtering Method Based on Cloth Simulation. *Remote Sens.* **2016**, *8*, 501. [CrossRef]
56. Anders, N.; Valente, J.; Masselink, R.; Keesstra, S. Comparing Filtering Techniques for Removing Vegetation from UAV-Based Photogrammetric Point Clouds. *Drones* **2019**, *3*, 61. [CrossRef]
57. Pinto, M.; Melo, A.G.; Honório, L.M.; Marcato, A.L.M.; Conceição, A.G.S.; Timotheo, A.O. Deep Learning Applied to Vegetation Identification and Removal Using Multidimensional Aerial Data. *Sensors* **2020**, *20*, 6187. [CrossRef] [PubMed]
58. Wang, Y.; Koo, K.-Y. Vegetation Removal on 3D Point Cloud Reconstruction of Cut-Slopes Using U-Net. *Appl. Sci.* **2022**, *12*, 395. [CrossRef]
59. Themistocleous, K. Themistocleous, K. The Use of UAVs for Cultural Heritage and Archaeology. In *Remote Sensing for Archaeology and Cultural Landscapes*; Chini, M., Ehlers, M., Lakshmi, V., Mueller, N., Refice, A., Rocca, F., Skidmore, A., Vadrevu, K., Eds.; Springer: Cham, The Netherlands, 2020; pp. 241–269. [CrossRef]
60. Zimmerman, D.; Pavlik, C.; Ruggles, A.; Armstrong, M.P. An experimental comparison of ordinary and universal Kriging and Inverse Distance Weighting. *Math. Geol.* **1999**, *31*, 375–390. [CrossRef]
61. Lu, G.Y.; Wong, D.W. An adaptive inverse-distance weighting spatial interpolation technique. *Comput. Geosci.* **2008**, *34*, 1044–1055. [CrossRef]
62. Dimple, D.; Rajput, J.; Al-Ansari, N.; Elbeltagi, A.; Zerouali, B.; Santos, C.A.G. Determining the Hydrological Behaviour of Catchment Based on Quantitative Morphometric Analysis in the Hard Rock Area of Nand Samand Catchment, Rajasthan, India. *Hydrology* **2022**, *9*, 31. [CrossRef]
63. Sassolas-Serrayet, T.; Cattin, R.; Ferry, M. The shape of watersheds. *Nat. Commun.* **2018**, *9*, 3791. [CrossRef] [PubMed]